Three-dimensional particle-in-cell simulations of energetic electron generation and transport with relativistic laser pulses in overdense plasmas

Y. Sentoku,[1] K. Mima,[1] Z. M. Sheng,[1] P. Kaw,[2] K. Nishihara,[1] and K. Nishikawa[3]
[1]*Institute of Laser Engineering, Osaka University, Suita, Osaka, Japan*
[2]*Institute for Plasma Research, Bhat, Gandhinagar, India*
[3]*Faculty of Engineering, Kinki University, Higashihirosima, Hiroshima, Japan*
(Received 30 August 2001; published 28 March 2002)

The interaction of relativistic laser light with overdense plasmas is studied by three-dimensional particle-in-cell simulations. Generation of layered current sheets and quasistatic magnetic fields is observed near the target surface owing to anisotropic laser filamentation and Weibel instabilities. Later these current sheets tear into filaments that partially merge with each other to form isolated magnetic channels penetrating into the dense plasmas. It is found that fast electron energy flow is not only inside the magnetic channels but also it is widely distributed outside the channels. This is possible because of electron anomalous diffusion across self-generated magnetic fields. Consequently, the total hot electron current exceeds a few hundred kiloamperes and is much larger than the Alfvén current. Hence a considerable amount of energy flows towards the plasma core. Significant heating of the bulk plasma electrons is also observed.

DOI: 10.1103/PhysRevE.65.046408 PACS number(s): 52.38.−r, 52.35.Qz, 52.65.Kj, 52.65.Rr

I. INTRODUCTION

In recent years, the advent of multiterawatt lasers capable of producing focused laser intensities over 10^{19} W/cm^2 and driving electron motion into the relativistic regime, has opened up many new interesting fields of research such as fast ignition for inertial fusion [1], development of novel high energy particle accelerators, short pulse x ray and neutron sources, etc. In the fast ignitor scheme, the intense laser pulse propagates through a coronal plasma up to several times the critical density and delivers energy to relativistic particles; these highly energetic particles then transport the energy through the overdense plasma to the center of the compressed core and ignite the fuel there. Considerable experimental and numerical simulation work has been done on the physics of intense laser pulse propagation and the acceleration of electrons and ions in high density plasmas. However, the related problem of the propagation of intense electron bunches into the core, has not received as much attention. It has only recently been realized that collective phenomena play a crucial role in this energy transport. This paper is devoted to a three-dimensional (3D) particle-in-cell (PIC) simulations of these collective phenomena.

Typically, the electron currents generated near the vacuum plasma interface exceed the Alfvén critical current [2], which should produce intense self-consistent B fields bending the electron trajectories backwards and preventing their penetration into the overdense plasma. However, in a dense plasma important shielding effects arise and the high energy electron current is neutralized by a cold electron return current. This allows the high energy electrons to propagate unimpeded into the overdense plasma. However, this system is unstable to a relativistic electromagnetic two-stream instability (the so-called Weibel instability [3]), which breaks up the fast electron current into filaments. 2D-PIC simulations have already shown the break up of fast electron beams into filaments guided by quasistatic magnetic fields [4,5]. The work of our group [6] and the more detailed work of Honda *et al.* [7] has shown that the current filaments are self-organized to a state in which each filament carries a net current less than the Alfvén limit. In this paper, we extend these works to the three-dimensional case with the help of 3D particle simulation. It is found that shallower magnetic channels are formed in the overdense regions and that the total magnetic energy is much lower than the total electron energy. Furthermore strong longitudinal electric fields are observed at the magnetic channel front and they play an important role in anomalous stopping and heating of the bulk plasma electrons. Also it is found that the merging time is proportional to the whistler mode period and varies as the cubic power of the size of the filament. The model of merging process is discussed.

This paper is organized as follows. Section II presents the results of the 3D-PIC simulations and a detailed description of the magnetic channel formation and the electron energy transport. The model of merging process is also discussed in the last part of Sec. II. Section III is devoted to the conclusion of this paper.

II. 3D-PIC SIMULATION OF ENERGETIC ELECTRON TRANSPORT IN OVERDENSE PLASMAS

A. Parameters of 3D-PIC simulations

Following are the simulation conditions. The target plasma is homogeneous, except for two longitudinal sharp boundaries, and its density is four times critical density (n_c), which corresponds to 4.4×10^{21} cm^{-3} for laser wavelength $\lambda=1$ μm. The plasma consists of fully ionized deuterons (ion mass is $3680m_e$), and the initial electron and ion temperatures are set to 10 keV and zero, respectively. The linearly polarized laser is irradiated from the left boundary. It is transversely uniform and longitudinally semi-infinite, which rises up in three laser cycles with a Gaussian profile. The maximum of the normalized vector potential is a (equivalent to $eA/m_ec^2)=3.75$, which corresponds to $I_0=2$

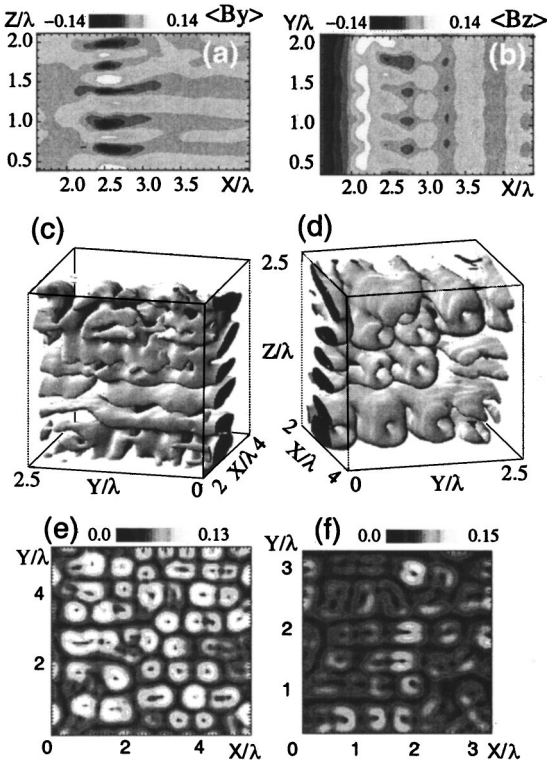

FIG. 1. Surface perturbation in early time stage. Longitudinal cut of transverse magnetic fields for $\langle B_y(B_z)\rangle$ in X-$Z(Y)$ plane (a) [(b)] [$Y(Z)=1.25\lambda$] at 8τ; Isosurface of quasistatic magnetic fields $\langle|B|\rangle=0.06B_0$ near laser irradiated surface at 16τ as viewed from the vacuum side (c) and from the target side (d); Contour plot of $|B|$ in the case of $n_e=4n_c(10n_c)$ and transverse $5(2.5)\lambda$ square at $t=16(12)\tau$ and at $2.7(1)\lambda$ from the surface (e) [(f)].

$\times 10^{19}$ W/cm^2 approximately, and an amplitude of the oscillating laser magnetic field $B_0=400$ MG. The transverse system size is $2.5\lambda\times 2.5\lambda$ and the longitudinal length is 12λ. The plasma has a length 8λ, and there are 2λ vacuum regions on both sides of the plasma. In this simulation, the coordinate X is longitudinal and Y and Z are transverse. Y is the laser polarization direction. Periodic boundary conditions are applied in the transverse direction. We assume an absorbing boundary for fields and a thermal reflection boundary for particles in X direction. The number of spatial grids and particles in the default parameter are $300\times 64\times 64$ and 2×10^7, respectively. The simulation has been run on Hitachi SR8000 using 4 GB main memory. Simulations with transverse $5\lambda\times 5\lambda$ and with the high density $10n_c$ have also been performed to check the periodic boundary effects on the scale of the filamentation.

B. Magnetic channel formation subsequent to the Weibel instability

Figure 1 shows the structure of quasistatic magnetic fields and the electromagnetic energy density at 6τ after laser irradiation, where τ is one laser oscillation period. Frame (a) shows $\langle B_y\rangle$ in the X-Z plane near the plasma surface (initial at $X=2\lambda$); here $\langle\ \rangle$ denotes time average over one laser period. The maximum growth rate of Weibel instability appears at a wave vector k such that $kc/\omega_p\sim 1$ [6]. It is seen that quasistatic magnetic fields with transverse scale length on the order of the local plasma skin depth $\lambda\simeq 2\pi\times c/\omega_p$ arise near the surface. These fluctuations, which find significant growth from noise within 10τ, can be attributed to the fastest growing modes of the Weibel instability, the growth rate is a few percent of the plasma frequency [6]. Figure 1(b) shows that similar structures are found in the $\langle B_z\rangle$ profile in the X-Y plane. The $\langle B_z\rangle$ fluctuations are relatively weaker than $\langle B_y\rangle$ fluctuations because the effective plasma temperature is anisotropic, being higher along the polarization direction (viz., Y direction) [6]. In addition to the Weibel instability of electrons, the modulational and filamentation instabilities of the laser pulse develop in the meantime. Specifically, the filamentation instability is found to be stronger in the direction perpendicular to the laser polarization direction. This arises from an anisotropic response of electrons to the transverse electric field as discussed by Nishihara *et al.* [8]. As a result, layered structures parallel to the laser polarization direction are formed, producing energetic electron flows in the same patterns as the laser intensity. This leads to the formation of magnetic neutral sheets. Figure 1(c) shows the isosurface $\langle B\rangle$ at $t=16\tau$ as observed from the laser irradiation direction . It is seen that the front of the magnetic neutral sheets soon break up into electron jets through a tearing and merging process in Y direction. Fig. 1(d) shows the same plot as in Fig. 1(c) but as observed from the overdense plasma side. For small scale filament formation ($kc/\omega_p\simeq 0.7, \omega_c\simeq 0.2\omega_0$), the time scale of tearing in the electron fluid is found to be of the order of the whistler mode period [10], which is $(\omega_c c^2k^2/\omega_p^2)^{-1}\sim 10/\omega_0$, where ω_p, ω_c, and ω_0 are plasma frequency, electron cyclotron frequency, and laser frequency, respectively. The magnetic fields increase drastically through the merging process after the tearing process. We notice that longitudinal components forming quadrupole structures around the x points are also excited.

Figure 1(e) shows the quasistatic magnetic structure at 16τ in the case with transverse $5\lambda\times 5\lambda$. The number of filaments is approximately the quadruple of those in Fig. 1(d). When the density is $10n_c$, both the time scale and the spatial scale are factor $\sqrt{4/10}$ as shown in Fig. 1(f). The filament density at 12τ in $10n_c$ plasma is about 1.5 times higher than that of the $4n_c$ case at 16τ. These results indicate that magnetic field structures are determined by physics and not by simulation size effects or the periodic boundary condition.

C. Shallower channel formation due to diffusive current distribution

Soon thereafter these magnetic filaments merge with each other into large scale filaments. The time scale of this merging process will be discussed later in Sec. II E. Figure 2 illustrates the build up of the coalescent filaments or channels, penetrating stably into the overdense plasma at $t=28\tau$. Figure 2(a) is the isosurface $\langle|B|\rangle=24$ MG of the quasistatic magnetic fields in the plasma region. Figs. 2(b) and (c) are transverse cuts of the forward and backward electron flows at $X=6\lambda$. Note that the forward electron flow is domi-

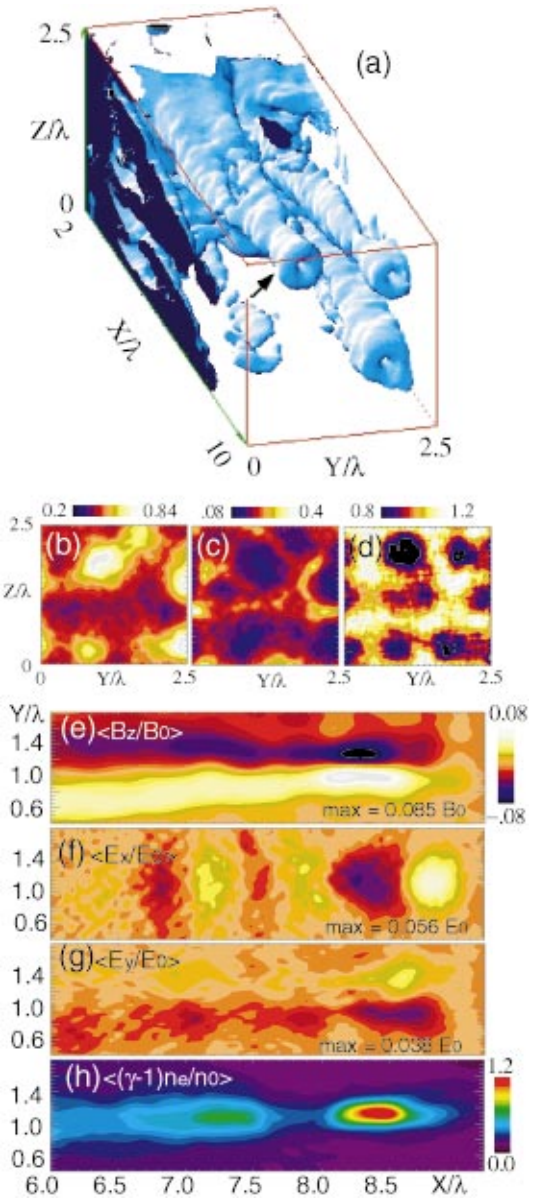

FIG. 2. (Color) 3D structure of magnetic channels at 28τ. (a) Isosurface of quasistatic magnetic fields $\langle|B|\rangle=0.06B_0$; (b) and (c) Transverse cuts of the energy density for electrons moving in the forward and backward directions at $X=6\lambda$, respectively; (d) Transverse cut of ion density at 40τ and $X=4\lambda$. The longitudinal X-Y cuts (at $Z=1.7\lambda$) of the channel indicated in frame (a) by an arrow are for (e) $\langle B_z/B_0\rangle$, (f) $\langle E_x/E_0\rangle$, (g) $\langle E_y/E_0\rangle$, and (h) $\langle(\gamma-1)n_e/n_0\rangle$, where E_0 (B_0),n_0 is the laser electric (magnetic) field and the initial target density, respectively.

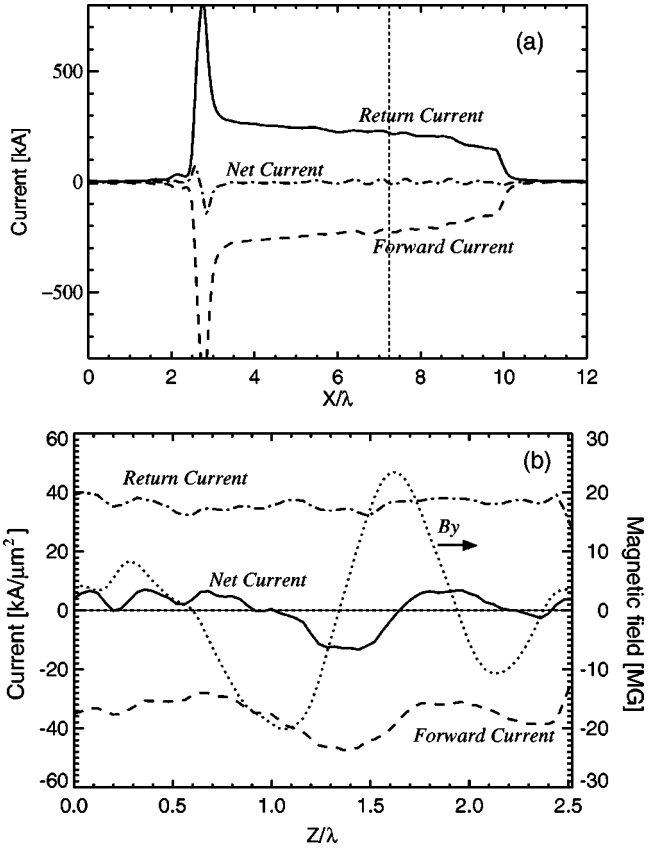

FIG. 3. (a) The longitudinal current profile integrated over the transverse region at $t=28\tau$. (b) The plot of the transverse currents profile with the magnetic field By at $(X,Y)=(7.2\lambda,0.8\lambda)$ indicated by the broken line in (a).

nant in the interior of the magnetic channels whereas, the return currents are dominant on the outside. This coaxial structure is similar to that shown in Ref. [7]. But in 3D case, the fast electron flow and the cold return flow are not separated clearly, namely, both the flows are found to be overlapping in wide regions and the current is well neutralized. In the channels, ion motion becomes obvious only on time scales $t\simeq 2\pi/\omega_{pi}$. Thus, it is noted that at $t\sim 40\tau$, about 20% of ions are evacuated from the channels by the electrostatic field [Fig. 2(d)] . We notice that the total energy of quasistatic magnetic field in overdense plasmas is only a few percent of the total electron energy in our 3D simulations. On the other hand, the total magnetic energy in 2D simulations by Honda *et al.* [7] is comparable to the total electron energy. The following is the reason why the magnetic field energy in 2D simulation is much higher than that of 3D simulation. In 3D simulation, the generated magnetic field near the surface of laser absorption are convected into overdense plasmas where the magnetic field is not strongly excited, while in 2D simulation, no convection loss of magnetic field energy is expected. An important quantitative result is that in the 3D simulations described here, the final structure of the channels is much shallower with low plasma evacuation and magnetic fields than those in the 2D simulations.

Figure 2(e) displays the longitudinal cut at the center of a magnetic channel. It is noted that the maximum magnetic fields of the channels is about $0.05B_0$ (20 MG) and the radius is ~ 0.5 μm, giving us an estimate of the current inside the channel to be about 5 kA. This is confirmed in the current profile shown in Fig. 3. The overall current neutralization in the transverse space is perfectly achieved as shown in Fig. 3(a). The total forward current (200 kA) is well neutralized by the return current and the total net current is almost zero in the overdense plasma. The incoming current from the sur-

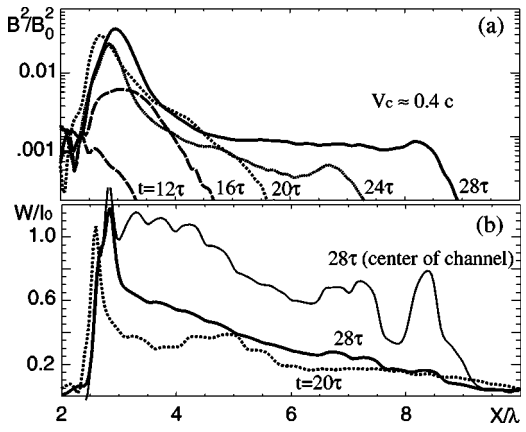

FIG. 4. (a) Time evolution of magnetic energy normalized by B_0^2; (b) Net energy flux W of electrons normalized by the laser peak intensity I_0. Both are averaged in Y and Z space.

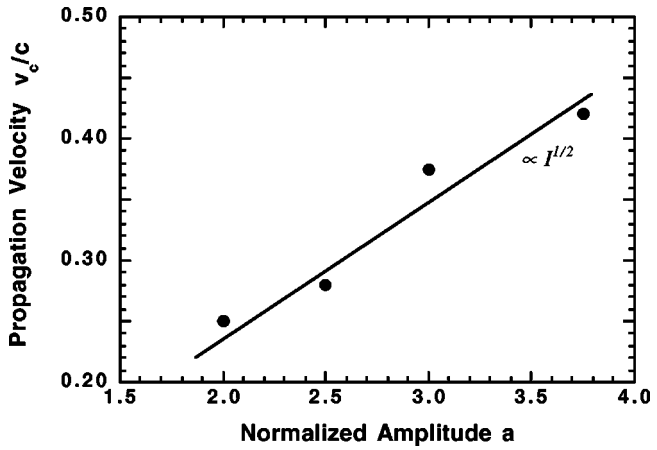

FIG. 5. The speed of the channel front versus the laser amplitude.

face reaches about 800 kA but the current is sharply dropped in a micron scale. This is because large numbers of hot electrons are prevented from penetrating into the plasma region by the intense magnetic fields near the surface shown in Fig. 4(a). In these magnetic fields, the larmor radius of a several hundreds keV electron is less than the channel radius (0.5 μm) and hence, such electrons are stopped. The hot electrons are also stopped by electric fields that have a double layer structure at the surface ($X\sim 3\lambda$). This electrostatic potential jump is about 200 keV in the present simulation.

In Fig. 3(b) it is found that the net current is a few kiloamperes inside the magnetic channel and this is much less than the Alfvén limit current [9] $I_A \simeq 17\beta_0\gamma_0$ kA$=30$ kA, here $\gamma_0\sim 2$ from the simulation results. However, the forward electron current in the channel (70 kA) exceeds the Alfvén limit current significantly. Furthermore, both the forward and return current is widely distributed in the transverse space, and they are not well separated, namely, the current neutralization works well. This is very important and very good feature to carry the fast electron energy into the plasma, means that although the net current inside a magnetic channel is small, the total hot electron current exceeds a few hundred kiloamperes and is much larger than the Alfvén limit current.

As for mechanisms of the formation of a cold electron distribution across magnetic field, there are a few possible mechanisms under investigation. One of them is the chaotic electron motion in return current. The orbit analysis indicates that backward electron motion is stochastic and induces anomalous resistivity. More details are discussed in Ref. [11].

Since there is time delay to neutralize current by cold electrons, the net current at the channel front is actually larger than that behind. As a result, the magnetic field (about $0.085B_0$) is higher at the channel front. Therefore, the electron flows are strongly pinched as shown in Figs. 2(e) and (h). Current and charge neutralization occurs in a time scale of electron response, or in a longitudinal space about $v_h/\omega_p \simeq c/\omega_p \sim 0.5$ μm, which is very close to the simulation result. Near the channel front, fast electrons excite large wakefieldlike electric fields, which accelerate electrons just behind the front and decelerate electrons at the front of the channel. Namely, the inductive electric fields are generated at the channel front by $\partial B_\theta/\partial t = -\partial E_\perp/\partial x + \partial E_x/\partial r$. These electric fields stop the fast electrons and heat the cold electrons.

Another interesting feature is concerned with the penetrating speed of the channel front. Figure 4(a) shows the time evolution of the magnetic energy distributions, averaged in transverse space. One observes that the energy density of the quasistatic magnetic field is very small, less than 0.1% B_0^2, at the early linear stage before $t=12\tau$, where B_0 is the incident magnetic field. It increases very quickly after $t=16\tau$ when the current sheets start to break up into filaments [Figs. 1(e) and (f)]. At $t=20\tau$ strong B fields with a peak amplitude about 70% ($\simeq 280$ MG) of B_0 are found at $X=3\lambda$.

When the magnetic field channels penetrate into the dense plasmas, the magnetic fields become weaker. The average magnetic fields are the order of 20 MG. The propagation speed of the front of magnetic channel is about $V_c=0.4c$. After running the code with the different laser intensity, we find that the speed of the channel front scales with the incident laser intensity like $I^{1/2}$, see Fig. 5. The channel front propagates as an electron magneto-hydrodynamic (EMHD) vortex with a speed given by [12]

$$\frac{V_c}{c} = \frac{1}{4\pi e n_h}\frac{\partial B_\theta}{\partial r} \simeq \frac{\omega_c}{\omega_0}\frac{1}{k_0 R_c}\frac{n_c}{n_h}, \tag{1}$$

following the Ampere's law, where n_h is the hot electron density at channel front, k_0 the wave number of the laser light and R_c the channel radius. Here we assume that the thermal pressure balances approximately between the hot and cold electrons at the channel boundary, i.e., $n_h T_h = n_{cold} T_c$. In the simulation $R_c=0.3\lambda$, $T_h/mc^2 \simeq 2$, $T_c/mc^2 \simeq 0.2$, $n_{cold} \simeq 4n_c$, and $\omega_c \simeq 0.3\omega_0$, then one obtains $n_h \simeq 0.4 n_c$ and $V_c \simeq 0.4c$, which is very close to the observation. Since $T_h \propto I^{1/2}$ according to simulations [13], one finds V_c scales like T_h, namely, by the square root of laser intensity, which agrees with our observation, if ω_c/T_c weakly depends on I.

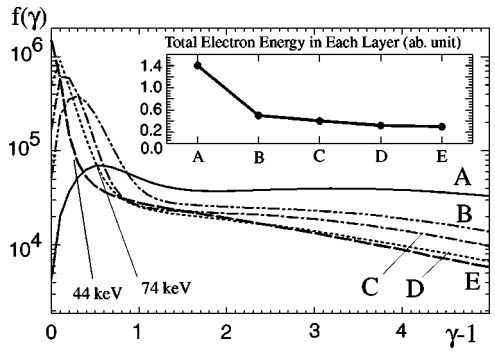

FIG. 6. Energy distributions of electrons in each layer at $t = 28\tau$. Inserted is the total electron energy in each layer.

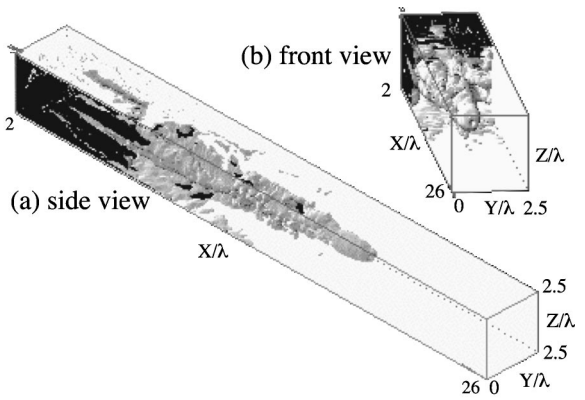

FIG. 7. Isosurface of quasistatic magnetic fields at 48τ. The plot level is same as that in Fig. 2(a), $\langle |B| \rangle = 0.06 B_0$.

D. Electron energy transport

The electron energy transport and deposition in overdense plasmas can be examined more explicitly by looking into spatial distribution of electron energy flux. Figure 4(b) is a longitudinal distribution of the net electron energy flux (averaged in a transverse section) at $t = 20\tau$ and 28τ. Throughout the simulation about 31.5% of the incident energy is absorbed at the plasma vacuum interface. Furthermore, about 20% of incident energy flux or 60% of absorbed energy passes through to the end of the channel at 28τ as shown in Fig. 4(b). The thin line is the energy flux at center of the channel [indicated by an arrow in Fig. 2(a)]. It drops sharply around $X \simeq 3\lambda$ due to intense magnetic field generation as discussed above, and then decreases gradually toward the channel front. It may be noted that a small number of electrons is decelerated inside the channel whereas, a considerably large number is stopped at the channel front by the longitudinal electric fields. The bulk plasma energy $\mathcal{E}$ increases with time according to the flux conservation law $\partial \mathcal{E}/\partial t + dW/dx = 0$, where W is the total energy flux. We can estimate from the gradient of the total flux that the heating rate is about $\partial T_e/\partial t \sim 40 \times (n_c/n_e)$ keV/fs. To see the energy deposition in the overdense plasma in more detail, we divide the simulated plasma region into five layers longitudinally. Each layer has a thickness of 1.6λ and they are labeled with A, B, C, D, and E at the rear sides of the layers, respectively. The electron energy distributions at $t = 28\tau$ on the boundaries of each layer are shown in Fig. 6, inserted in the figure is the electron energy in each layer at that time. It appears that intense magnetic fields strongly block the penetration of fast electrons at the surface and at the channel front whereas, in the interior of the magnetic channels, the penetration of fast electrons is impeded by collective processes which convert fast electron kinetic energy into bulk electron heating. Thus, the region E is heated up to about 44 keV from the initial plasma temperature in a few femtoseconds after the channel front arrival.

E. Discussion on merging process of filament

To investigate the process of merging of current channels over a long time period, we have performed a simulation with a long scale plasma (now three times longer than the case of Fig. 2). The filaments now continuously merge and disappear. We show snapshots of the current channel structure at 48τ in Figs. 7(a) and (b). Eventually, only one filament survives and continuously penetrates into the overdense plasma with almost constant velocity $V_c \sim 0.4c$ as discussed in Sec. II C. This section, we discuss the time scale of the merging process using incompressible electron fluid model.

Figures 8(a) and (b) illustrate the merging of two filaments each with area σ. As the two filaments approach each other with velocity u, the incompressibility of the electron fluid causes the electron flow inside the channel to be pushed aside with a velocity of order u. Consequently, longitudinal magnetic fields with a quadrupole structure are excited. Figure 8(c) shows an example of the generation of longitudinal magnetic fields in a 3D-PIC simulation of the merging process. Similar quadrupole structures have been reported in Ref. [14].

The Ampere's law, $-\partial B_x/\partial y = \mu_0 j_z$ and definition $j_z \equiv -e n_e u$, we get an expression for the merging velocity u as

$$u \simeq \frac{2\beta}{\sqrt{\sigma}} \frac{c^2}{\omega_p^2} \omega_c , \tag{2}$$

where we have replaced $|B_x|$ by $\beta |B_\theta|$ (with β, the ratio of the maximum longitudinal and transverse magnetic fields, of order 0.3 in the simulations) and taken $\partial/\partial y \sim 2/\sqrt{\sigma}$. Merging time is then approximately given by

$$\tau_M \simeq \frac{\sqrt{\sigma}}{u} = \left(2\beta \frac{c^2}{\omega_p^2} \omega_c \right)^{-1} \sigma . \tag{3}$$

We find that the merging period is proportional to the whistler mode period just as in the tearing times cale problem in Sec. II B.

The current is likely to remain constant during the merging process, we may write $\omega_c = \omega_{c,0}/\sqrt{\sigma/\sigma_0}$, where the subscript 0 refers to the parameters of the initial filament. Then, the merging period is proportional to the cubic of $\sqrt{\sigma}$,

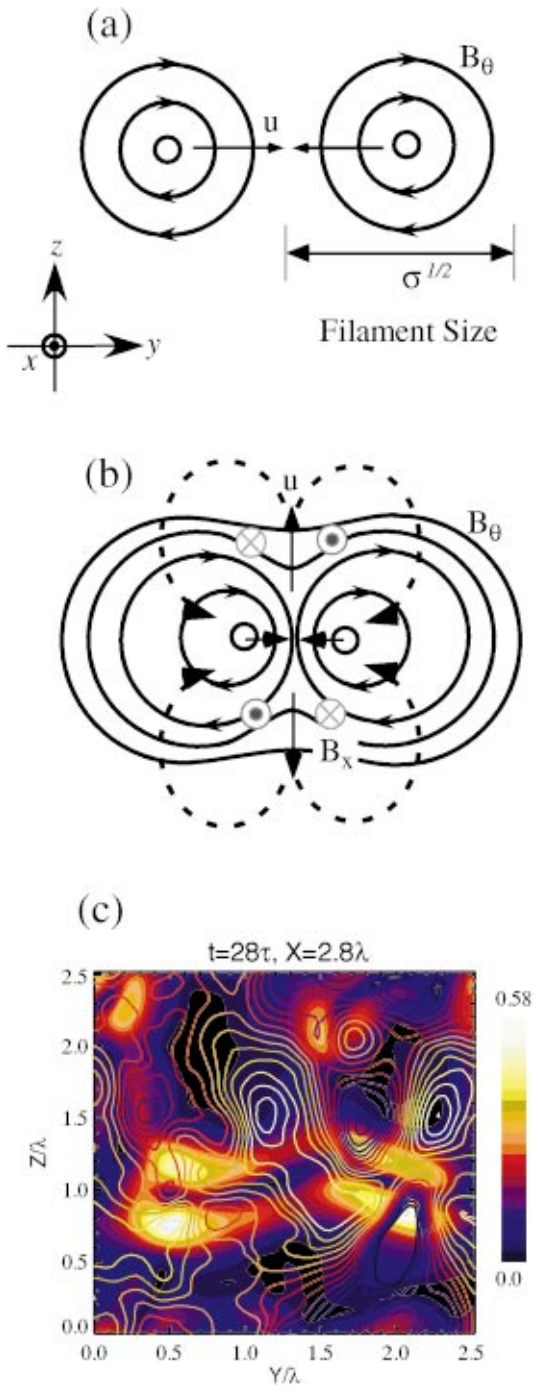

FIG. 8. (Color) The incompressible fluid model of merging process (a) and (b). The dense plot in (c) is the azimuthal magnetic fields and the contour lines indicate the longitudinal magnetic fields, which appear through the merging process. Plot in (c) is observed at $t=28\tau$ and $X=0.8\lambda$ inside the overdense plasma. The maximum longitudinal field is about 30% of the azimuthal field.

$$\tau_M = \alpha(\sigma)^{3/2}. \tag{4}$$

This means that the small scale filaments merge rapidly, while the large filaments merge more slowly and they are more stable.

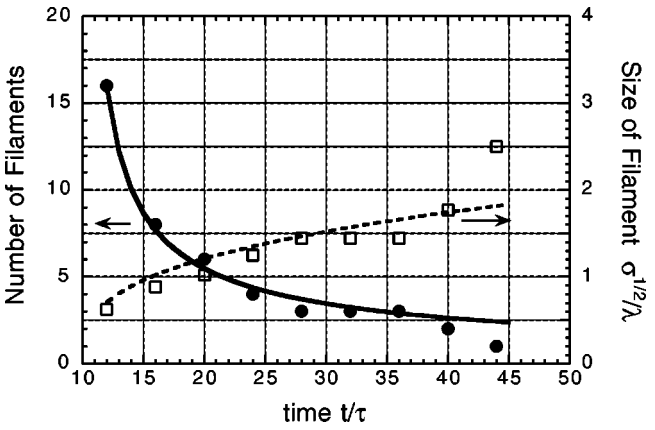

FIG. 9. Time evolution of the number and size of filaments. The simulation results are plotted with filled circles and the solid line is the prospect by Eq. (6). The blank squares indicate the size of the filaments in the simulation.

τ_M is the time taken for the number of filaments to decrease by a factor of 2, we may write a time evolution equation for the number of merging filaments as

$$\frac{dN}{dt} \equiv -\frac{\ln 2}{\tau_M} N, \tag{5}$$

number of filaments is also defined as $S \equiv \sigma$, where S is area of the simulation (2.5 μm square). Using Eq. (4) and the definition of N, Eq. (5) can give

$$N(t) = \frac{N_0}{\left\{1 + \dfrac{3 \ln 2 (t - t_0) N_0^{3/2}}{2 \alpha S^{3/2}}\right\}^{2/3}}. \tag{6}$$

Figure 9 shows the time evolution of the number in the simulation (filled circle) and Eq. (6) (solid line). $N(t)$ is plotted using $N_0 = 16$ and α was obtained fitting with the first two points $t = 12$ and 16 in the simulation. Number of filaments in the simulation agrees well with Eq. (6).

III. CONCLUSION

In conclusion, the formation and time evolution of quasistatic magnetic channels during the interaction of an ultraintense laser with an overdense plasma has been demonstrated for the first time using a 3D-PIC simulation. It is found that the electron energy transport is inhibited near the irradiated surface due to intense quasistatic magnetic fields and double layerlike E field generated on the surface. However, various collective effects form stable magnetic channels in overdense plasmas, and these channels sustain high flux of fast electron, which is much larger than the Alfvén limit current. Namely, the fast electron current is effectively neutralized by a return current of cold electrons everywhere in the dense plasma. These features are quite different from the previous 2D simulations and are first demonstrated by 3D-PIC simulations in this paper.

The propagation speed of magnetic channel front is

slower than the speed of fast electrons and can be explained by an EMHD vortex propagation model. Inside the magnetic channels the MeV electrons are stopped via collective processes in several micrometers and the background plasma is heated up to hundred keV in several tens of laser periods.

The merging period is found to be proportional to the whistler mode period and also cubic of the filament size. The model agrees well with what we observed in the 3D-PIC simulations.

ACKNOWLEDGMENTS

The authors acknowledge helpful discussions with S. V. Bulanov, T. Taguchi, M. Honda, and H. Ruhl. Also Y.S. would like to thank the computational staffs of ILE and CyberMedia Center of Osaka University. P.K., K.N., and K.M. are supported by a Grant-in-Aid for Scientific Research for the Ministry of Education, Science, Sport and Culture of Japan.

[1] M. Tabak *et al.*, Physica B **1**, 1626 (1994).
[2] H. Alfvén, Phys. Rev. **55**, 425 (1939).
[3] E.S. Weibel, Phys. Rev. Lett. **2**, 83 (1959).
[4] A.M. Pukhov and J. Meyer-ter-Vehn, Phys. Rev. Lett. **79**, 2686 (1997); Phys. Plasmas **5**, 1880 (1998).
[5] B.F. Lasinski *et al.*, Phys. Plasmas **6**, 2041 (1999).
[6] Y. Sentoku *et al.*, Phys. Plasmas **7**, 689 (2000).
[7] M. Honda, J. Meyer-ter-Vehn, and A. Pukhov, Phys. Plasmas **7**, 1302 (2000).
[8] K. Nishihara *et al.*, Proc. SPIE **3886**, 90 (1999).
[9] D.A. Hammer and N. Rostoker, Phys. Fluids **13**, 1831 (1970).
[10] A. Fruchtman and H.R. Strauss, Phys. Fluids B **5**, 1408 (1993).
[11] Y. Sentoku *et al.*, Proceedings of the Second International Conference on Intertial Fusion Sciences and Application (to be published).
[12] A. Das, Plasma Phys. Controlled Fusion **41**, A531 (1999); P. G. Saffman, *Vortex Dynamics* (Cambridge University Press, Cambridge).
[13] S.C. Wilks *et al.*, Phys. Rev. Lett. **69**, 1383 (1992); Y. Sentoku *et al.*, Phys. Plasmas **5**, 4366 (1998).
[14] M. Honda *et al.*, Phys. Rev. Lett. **85**, 2128 (2000).